Neutrino-induced neutron spallation and supernova *r*-process nucleosynthesis

Y.-Z. Qian,[1] W. C. Haxton,[2] K. Langanke,[3,4] and P. Vogel[1]
[1]*Department of Physics, 161-33, California Institute of Technology, Pasadena, California 91125*
[2]*Institute for Nuclear Theory, Box 351550, University of Washington, Seattle, Washington 98195*
and Department of Physics, Box 351560, University of Washington, Seattle, Washington 98195
[3]*W. K. Kellogg Radiation Laboratory, 106-38, California Institute of Technology, Pasadena, California 91125*
[4]*Institute of Physics and Astronomy, University of Aarhus, Denmark*
(Received 5 November 1996)

It is quite likely that the site of the *r* process is the hot, neutron-rich ''bubble'' that expands off a proto-neutron star during a core-collapse supernova. The *r* process would then occur in an intense flux of neutrinos. In order to explore the consequences of the neutrino irradiation, we calculate the rates of charged-current and neutral-current neutrino reactions on neutron-rich heavy nuclei, and estimate the average number of neutrons emitted in the resulting spallation. Our results suggest, for a dynamic *r* process occurring in an expanding bubble, that charged-current ν_e captures might help shorten the time scale for the *r* process, bringing it into better accord with our expectations about the conditions in the hot bubble: neutrino reactions can be important in breaking through the waiting-point nuclei at $N=50$ and 82, while still allowing the formation of abundance peaks. Furthermore, after the *r* process freezes out, there appear to be distinctive neutral-current and charged-current postprocessing effects. These include a spreading of the abundance peaks and damping of the most pronounced features (e.g., peaks and valleys) in the unpostprocessed abundance distribution. Most importantly, a subtraction of the neutrino postprocessing effects from the observed solar *r*-process abundance distribution shows that two mass regions, $A=124$–126 and 183–187, are inordinately sensitive to neutrino postprocessing effects. This imposes very stringent bounds on the freeze-out radii and dynamic time scales governing the *r* process. Moreover, we find that the abundance patterns within these mass windows are entirely consistent with synthesis by neutrino interactions. This strongly argues that the *r* process must occur in the intense neutrino flux provided by a core-collapse supernova. It also greatly restricts dynamic models for the supernova *r*-process nucleosynthesis. [S0556-2813(97)02803-3]

PACS number(s): 26.30.+k, 13.15.+g, 25.30.Pt, 95.30.Cq

I. INTRODUCTION

It is known that approximately half of the heavy elements with $A>70$ and all of the transuranics are formed by the process of rapid neutron capture, the *r* process. The astrophysical site where the required conditions for the *r* process are produced—neutron number densities in excess of $\sim 10^{20}$ cm^{-3} and temperatures of $\sim 10^9$ K lasting for on the order of 1 s [1]—has been a matter of continuing speculation. Recently, it has been argued that an attractive and plausible site is the ''hot bubble'' that expands off the proto-neutron star during a core-collapse supernova [2]. Neutron-rich matter initially composed of free nucleons is blown off the neutron star. As this nucleon soup expands and cools, almost all the protons are locked into α particles. Then an α process takes place to burn α particles into seed nuclei with A close to 100 [3]. The *r* process occurs through the capture of the excess neutrons on these seed nuclei. Although numerical calculations of this process fail in some aspects, both the produced *r*-process abundance distribution and the amount of *r*-process material ejected per supernova are roughly in accord with observation [2].

If the *r* process occurs near the protoneutron star, within perhaps 1000 km, then it takes place in an intense flux of neutrinos of all flavors emitted by the cooling neutron star. In this paper we study the effects of charged-current and neutral-current neutrino reactions with neutron-rich heavy nuclei during and following the *r* process. Neutrino reactions can affect the *r*-process nucleosynthesis in two ways, by driving nuclear transitions that alter the path or pace of the *r* process, or by modifying the abundance pattern through neutrino-induced neutron spallation after the *r* process is completed. During the *r* process perhaps the most interesting possibility is charged-current ν_e capture at a rate competitive with β decay, which would therefore speed up the nuclear flow from one isotopic chain to the next of higher Z [4]. This could be quite helpful in accelerating the passage through the closed-neutron-shell nuclei at $N=50$ and 82, as conventional waiting times of several seconds are perhaps a bit troublesome in relation to the shorter hydrodynamic time scales for the hot bubble. (Note, however, the nuclear flow through the $N=50$ closed neutron shell may be carried by α-capture reactions during the α process preceding the *r* process as in the particular scenario of Woosley *et al.* [2].) On the other hand, it is clear that the existence of abundance peaks at $A\sim 80$, 130, and 195 places some constraints on this possibility: these peaks are clear signatures that slow waiting-point β decay rates are controlling the nuclear flow at the time the *r* process freezes out [5]. By comparing the β decay rates with the flux-dependent ν_e capture rates, Fuller and Meyer [6] showed that the individual abundance peaks have to be made at sufficient distances above the neutron star. In our study we have extended their work and that of McLaughlin and Fuller [7] by quantitatively considering the competition

between β decay and charged-current neutrino reactions in the context of a dynamic, expanding bubble in order to more realistically determine what role neutrinos may play in the nuclear flow.

However, our present work is mainly concerned with the postprocessing of the r-process abundance distribution by neutrino-induced neutron spallation. Apart from the study of Domogatskii and Nadëzhin [8], who estimated production yields for certain bypassed isotopes from charged-current neutrino spallation reactions, little work has been done on this possibility. In our present study we find that the spallation following charged-current and neutral-current neutrino excitation of nuclei can have a number of effects on r-process yields: abundance peaks can be shifted and broadened, minima in the abundance pattern can be filled, and the unevenness of yields can be smoothed in a characteristic way. But most importantly, one can demonstrate directly from the neutrino physics calculations and the known r-process abundance distribution that two mass windows, $A=124-126$ and 183–187, are inordinately sensitive to neutrino postprocessing. This imposes new and stringent bounds on the freeze-out radii and dynamic time scales in the supernova r-process models. Moreover, the pattern of abundances within these windows is entirely consistent with neutrino-induced synthesis. Unless this is an unfortunate and accidental result, it would appear to provide direct proof that the r process occurs in an intense neutrino fluence, i.e., in a core-collapse supernova. Further knowledge of postprocessing neutrino fluences greatly reduces the freedom in dynamic models of the r process, explicitly relating, for example, the dynamic time scale to the conditions at freeze out. These results take on added significance because the neutrino physics of a core-collapse supernova is generally believed to be far less model dependent than the hydrodynamics.

In this paper we also calculate the nuclear physics input for the postprocessing and other possible effects of neutrinos on the r process. We present detailed estimates of the charged-current ν_e capture rates using both empirical data and the shell model, the comparison of which provides some measure of the nuclear structure uncertainties. Previous studies of ν_e capture on heavy nuclei have been carried out by Fuller and Meyer [6], and by McLaughlin and Fuller [9]. The continuum random phase approximation (CRPA) and shell-model techniques are employed in the calculations of neutral-current cross sections. The subsequent decay of the highly excited nuclei by neutron emission is estimated by the statistical Hauser-Feshbach techniques. We stress that the distinctiveness of the neutrino postprocessing signals can be traced to well-understood aspects of nuclear structure, such as the tendency of highly excited neutron-rich nuclei to emit multiple neutrons.

II. CALCULATIONS OF NEUTRINO-NUCLEUS INTERACTION PROCESSES

The rate for a specific neutrino reaction at a distance r from the center of the neutron star can be expressed in convenient units as

$$\lambda_\nu \approx 4.97\left(\frac{L_\nu}{10^{51}\ \text{erg s}^{-1}}\right)\left(\frac{\text{MeV}}{\langle E_\nu\rangle}\right) \times\left(\frac{100\ \text{km}}{r}\right)^2\left(\frac{\langle\sigma_\nu\rangle}{10^{-41}\ \text{cm}^2}\right)\ \text{s}^{-1}, \tag{1}$$

where L_ν and $\langle E_\nu\rangle$ are the luminosity and average energy, respectively, of the neutrino species responsible for the reaction, and $\langle\sigma_\nu\rangle$ is the corresponding cross section averaged over the neutrino spectrum. The spectrum-averaged neutrino reaction cross section is

$$\langle\sigma_\nu\rangle=\sum_f\int\sigma_\nu^f(E_\nu)f_\nu(E_\nu)dE_\nu, \tag{2}$$

where the sum extends over all possible final nuclear states f. The neutrino spectrum in the above equation, $f_\nu(E_\nu)$, is taken to be

$$f_\nu(E_\nu)=\frac{1}{F_2(\eta_\nu)T_\nu^3}\frac{E_\nu^2}{\exp[(E_\nu/T_\nu)-\eta_\nu]+1}, \tag{3}$$

where T_ν and η_ν are parameters fitted to numerical spectra, and $F_2(\eta_\nu)$ normalizes the spectrum to unit flux. The transport calculations of Janka [10] yield spectra with $\eta_\nu\sim 3$ for all neutrino species. While this choice also provides a good fit to the ν_e and $\overline{\nu_e}$ spectra calculated by Wilson and Mayle, their heavy-flavor neutrino spectra have approximately a black-body shape ($\eta_\nu\sim 0$) [11]. In this work we take $\eta_{\nu_e}=3$ and $\eta_{\nu_{\mu(\tau)}}=\eta_{\overline{\nu}_{\mu(\tau)}}=0$, though we also have done calculations with other choices of η_ν. The average neutrino energy is given by $\langle E_\nu\rangle\approx 3.99T_\nu$ for $\eta_\nu=3$ and $\langle E_\nu\rangle\approx 3.15T_\nu$ for $\eta_\nu=0$.

The neutrino interactions of interest are charged-current ν_e and neutral-current $\nu_{\mu(\tau)}$ and $\overline{\nu_{\mu(\tau)}}$ reactions on the waiting-point nuclei in the r process. For the very neutron-rich heavy nuclei in the r process, charged-current $\overline{\nu_e}$ reactions can be neglected because allowed transitions are Pauli blocked. For typical average supernova neutrino energies $\langle E_{\nu_e}\rangle\approx 11$ MeV, $\langle E_{\overline{\nu}_e}\rangle\approx 16$ MeV, and $\langle E_{\nu_{\mu(\tau)}}\rangle \approx\langle E_{\overline{\nu}_{\mu(\tau)}}\rangle\approx 25$ MeV, the heavy-flavor neutrinos dominate neutral-current reaction rates. (Clearly the corresponding charged-current $\nu_{\mu(\tau)}$ reactions are energetically prohibited.)

Thus the task before us is to estimate the relevant cross sections for an appropriate range of neutrino energies and final nuclear states, so that Eq. (2) can be evaluated. In principle this could be done explicitly for each nucleus involved in the r-process network, using some technique such as the CRPA or the shell model. But this approach is clearly impractical numerically. Instead, we present in this section a more schematic description of the cross sections, one largely based on experimental systematics. Our strategy is then to check this phenomenological approach with explicit CRPA and shell-model calculations for a few test nuclei.

At typical supernova neutrino energies the dominant contribution to the total cross section for ν_e capture on a parent nucleus with charge Z comes from the allowed transitions to the isobaric analog state (IAS) and the Gamow-Teller (GT) resonance states in the daughter nucleus. The allowed cross section is

$$\sigma(E_{\nu_e})=\frac{G_F^2\cos^2\theta_c}{\pi}\,k_eE_eF(Z+1,E_e)\times[|M_F|^2+(g_A^{\rm eff})^2|M_{GT}|^2], \quad (4)$$

where G_F is the Fermi constant, E_e and k_e the energy and three-momentum of the outgoing electron, respectively, θ_c the Cabibbo angle, and $F(Z+1,E_e)$ a correction for the Coulomb distortion of the outgoing electron wave function. The relativistic form of $F(Z,E_e)$ is used in evaluating the integral in Eq. (2). We also use an effective axial-vector coupling constant $g_A^{\rm eff}=1$, rather than the bare nucleon value 1.26, a renormalization that improves the agreement between shell-model studies and experiments in the $2s1d$ and $2p1f$ shells [12].

The allowed Fermi and GT transition strengths are

$$|M_F|^2=\frac{1}{2J_i+1}|\langle J_f||\sum_{i=1}^{A}\tau_+(i)||J_i\rangle|^2 \quad (5)$$

and

$$|M_{\rm GT}|^2=\frac{1}{2J_i+1}|\langle J_f||\sum_{i=1}^{A}\sigma(i)\tau_+(i)||J_i\rangle|^2, \quad (6)$$

respectively. To evaluate Eq. (2) we must specify the distribution of these transition probabilities over the final states of the daughter nucleus.

In the limit of good isospin the Fermi strength $|M_F|^2=N-Z$ is carried entirely by the IAS in the daughter nucleus. The excitation energy of the IAS, relative to the parent ground state, can be estimated quite accurately from the Coulomb energy difference [6]

$$E_{\rm IAS}\approx\frac{1.728Z}{1.12A^{1/3}+0.78}-1.293\ \ {\rm MeV}. \quad (7)$$

The total GT strength is also simple due to the fact that the nuclei of interest have large neutron excesses, effectively eliminating all strength in the $(\overline{\nu_e},e^+)$ channel. It follows that the strength in the (ν_e,e^-) channel is given by the Ikeda sum rule, $\Sigma_f|M_{\rm GT}|^2\approx 3(N-Z)$. However, the distribution of this GT strength is not determined by general arguments and thus must be either calculated or measured. Studies using forward-angle (p,n) scattering with stable targets have shown that most of the strength is concentrated in a broad resonance whose center is in the vicinity of the IAS. This motivated us to approximate the GT-strength distributions for the nuclei of present interest as Gaussians centered at $E_{\rm GT}$ and with a full width at half maximum $\Gamma=2(\ln 2)^{1/2}\Delta$,

$$|M_{\rm GT}(E)|^2\sim S\,\exp[-(E-E_{\rm GT})^2/\Delta^2]. \quad (8)$$

That is, we represent the distribution of $|M_{\rm GT}|^2$ summed over all final states—both discrete bound states and continuum states—by the continuous function $|M_{\rm GT}(E)|^2$ of Eq. (8). The normalization constant S is fixed by the condition that Eq. (8), integrated over all excitation energies $E\geq E_{\rm gs}$, where $E_{\rm gs}$ is the ground-state energy of the daughter nucleus, gives the sum rule result $3(N-Z)$. This representation of the GT-strength distribution may have been first introduced many years ago in the so-called gross theory of β decay. It has been used in β-decay and neutrino reaction studies many times since, e.g., in the recent study of ν_e capture on heavy nuclei by McLaughlin and Fuller [9]. We have taken the Gaussian centroids $E_{\rm GT}$ from the analytic fit to $\delta=E_{\rm GT}-E_{\rm IAS}$ in Ref. [13], where GT-strength distributions from forward-angle (p,n) measurements were studied. While the measurements are confined to nuclei near stability, the data show that δ is linearly correlated with $N-Z$, leading to the prediction that $\delta\sim 0$ for the neutron-rich nuclei of present interest. We took $\Gamma\sim 5$ MeV which is also a value typical of the (p,n)-measured GT-strength profiles.

Following the prescription outlined above, we have calculated the rates for ν_e captures on the waiting-point nuclei with $N=50$, 82, and 126 in the r process, using an average ν_e energy of $\langle E_{\nu_e}\rangle\approx 11$ MeV. The rates for $L_{\nu_e}=10^{51}$ erg s^{-1} at a radius of $r=100$ km are given in Table I. These rates can be easily scaled for different L_{ν_e} and r using Eq. (1).

Such ν_e reactions typically excite the daughter nucleus to states with excitation energies of ~ 20 MeV, which is well beyond particle breakup threshold. Because these nuclei are very neutron-rich, they deexcite by emitting several neutrons, a process we have simulated using a statistical neutron evaporation code [14]. This code estimates the average number of neutrons emitted by these nuclei $\langle n\rangle$ as well as the probabilities for emitting any specific number of neutrons (e.g., $P_{n=2}$), quantities that will be important in our postprocessing calculations. Nuclear masses, which are generally not known experimentally, have been taken from the compilation of Möller *et al.* [15]. As expected from the average neutron separation energies at the $N=50$, 82, and 126 shell closures, we find that there are about 2–5 neutrons emitted after each ν_e capture on the waiting-point nuclei (see Table I).

Neutral-current neutrino-nucleus interactions in supernovae have been studied previously in Refs. [16,17]. As in the charged-current case, there is an allowed contribution. The operator analogous to the Fermi operator contributes only to elastic neutrino scattering, and hence is of no interest. Thus inelastic allowed transitions are governed by the neutral-current GT transition probability

$$|M_{\rm GT}^{\rm NC}|^2=\frac{1}{2J_i+1}|\langle J_f||\sum_{i=1}^{A}\sigma(i)\frac{\tau_3(i)}{2}||J_i\rangle|^2. \quad (9)$$

We use the same renormalized $g_A^{\rm eff}$ as in the charged-current case for the neutral-current GT transitions. In the calculations described below, we found that most of this strength was concentrated below or very close to the neutron emission threshold, resulting in a relatively modest contribution to the neutron spallation channels of present interest.

Because $\nu_{\mu(\tau)}$ and $\overline{\nu}_{\mu(\tau)}$ have a higher mean energy, odd-parity transitions generated by first-forbidden operators—those proportional either to the momentum transfer or to nucleon velocities—must be considered. (For the ν_e spectrum employed here, the contribution of first-forbidden transitions to the charged-current ν_e capture rates is known to be small from, for example, the shell-model calculations in Ref. [16], which included all contributing multipoles.) One pro-

TABLE I. Results for ν_e capture on the waiting-point nuclei in the r process. The ν_e capture rates $\lambda_\nu^{\mathrm{CC}}$ are calculated with $\langle E_{\nu_e}\rangle \approx 11$ MeV, $\eta_{\nu_e} \approx 3$, and $L_{\nu_e} = 10^{51}$ erg s^{-1} at $r = 100$ km, under the assumption of a Gaussian GT-strength distribution with a full width at half maximum of $\Gamma \approx 5$ MeV. The last seven columns give $\langle n\rangle$, the average number of neutrons emitted after a ν_e capture reaction, and various probabilities for multiple neutron emission.

Z	N	A	$\lambda_\nu^{\mathrm{CC}}$ (s^{-1})	$\langle n\rangle$	$P_{n=1}$	$P_{n=2}$	$P_{n=3}$	$P_{n=4}$	$P_{n=5}$	$P_{n=6}$
26	50	76	8.1	3.1	0	0.06	0.83	0.08	0.02	0
27	50	77	7.0	2.9	0	0.11	0.83	0.06	0	0
28	50	78	6.0	2.0	0	0.88	0.12	0	0	0
29	50	79	5.1	2.0	0	0.92	0.08	0	0	0
30	50	80	4.3	1.9	0.11	0.89	0	0	0	0
31	50	81	3.7	1.8	0.19	0.81	0	0	0	0
31	52	83	4.5	2.0	0.02	0.89	0.09	0	0	0
45	82	127	7.3	3.0	0	0.03	0.91	0.06	0	0
46	82	128	6.5	2.6	0	0.32	0.68	0	0	0
47	82	129	5.8	2.5	0	0.45	0.55	0	0	0
48	82	130	5.2	2.1	0	0.83	0.17	0	0	0
49	82	131	4.6	2.0	0	0.90	0.10	0	0	0
49	84	133	5.3	3.0	0	0.04	0.95	0.01	0	0
65	126	191	10.1	5.1	0	0	0	0.10	0.75	0.15
66	126	192	9.3	4.6	0	0	0	0.42	0.58	0
67	126	193	8.5	4.6	0	0	0	0.38	0.62	0
68	126	194	7.8	4.0	0	0	0.08	0.83	0.09	0
69	126	195	7.2	4.0	0	0	0.06	0.89	0.05	0

cedure [16] for estimating the first-forbidden contribution to neutral-current neutrino scattering is the generalized Goldhaber-Teller model, which satisfies the Thomas-Reiche-Kuhn (TRK) sum rule for $E1$ transitions as well as its generalization for first-forbidden multipoles of the axial current [18]. The strengths are carried by doorway states placed in the center of the giant resonance region. The TRK sum rule predicts a response proportional to $NZ/A = (A/4)\{1 - [(N-Z)/A]^2\}$. Even for the neutron-rich nuclei in the r process, $NZ/A \approx A/4$ is good within $\sim 10\%$. Therefore, if the first-forbidden contribution proves important, one expects the total heavy-flavor neutral-current cross section to scale as

$$\langle \sigma_\nu^{\mathrm{NC}} \rangle \approx \sigma_0 A, \tag{10}$$

where $\sigma_0 \approx 10^{-42}$ cm^2 for $\langle \underline{E}_\nu \rangle \approx 25$ MeV when averaged over, for example, ν_μ and $\underline{\nu}_\mu$. This was the case for the calculations done in Ref. [16], and it also was found to hold in our estimates of the cross section above neutron emission threshold for nuclei of interest to the r process.

We have tried to assess the accuracy of our various cross section estimates by performing CRPA and shell-model ''benchmark'' calculations. The shell-model study was done for the waiting-point nucleus ^{78}Ni and its daughter ^{78}Cu in the (ν_e, e^-) reaction. We employed a modified Kuo g matrix (originally intended for the ^{56}Ni region, but rescaled by 0.8 to account for the larger mass numbers of interest here), supplemented by the Sussex potential matrix elements in those cases involving the $1g_{7/2}$ shell. The charged-current GT response was evaluated from the naive ^{78}Ni closed-shell ground state to a complete set of ^{78}Cu final states including, for example, those with a hole in the $1f_{7/2}$ shell or a particle in the $1g_{7/2}$ shell. While this basis is somewhat simple, it has the virtue that the Ikeda sum rule is exhausted by the (ν_e, e^-) channel; thus this calculation is compatible with the assumptions made in our schematic treatment above. The distribution of the transition probability $|M_{\mathrm{GT}}|^2$ was evaluated in this shell-model basis by a method of moments, rather than by a state-by-state summation. A least-squares best fit to the results using the function in Eq. (8) was then made in order to determine shell-model values for the parameters E_{GT} and Γ.

The results are reasonably satisfying. The shell model yielded $\delta = E_{\mathrm{GT}} - E_{\mathrm{IAS}} = -3.36$ MeV, which can be compared with the result of -1.15 MeV one obtains by extrapolating the fit of Ref. [13]. Thus the prediction of this fit that the centroid of the GT-strength distribution should fall below the IAS for the neutron-rich nuclei of present interest is confirmed by the shell-model calculation. While there is a difference of ~ 2 MeV in the precise location of the centroid, this is not very significant for our neutrino cross sections: a shift of 2 MeV either way in the centroid changes the cross sections by less than $\sim 50\%$.

The shell-model prediction for Γ, 11.7 MeV, is not in good agreement with the assumed value of 5 MeV, which we argued was typical of fits to GT-strength profiles deduced from (p,n) forward scattering. Because the neutrino cross sections are quite insensitive to Γ [9], the origin of this discrepancy is a somewhat academic issue. Nevertheless, these results motivated us to perform analogous calculations for ^{64}Ni, a stable target for which the (p,n)-deduced GT-strength distribution is known [19]. Again the shell-model prediction of $\delta \sim 5$ MeV was in good agreement with the prediction of 3.4 MeV by the fit of Ref. [13], as well as with the data. Yet the shell model yielded a less distinct resonance

TABLE II. Some illustrative results for neutral-current neutrino interactions from CRPA calculations. The cross sections (per heavy-flavor neutrino species) above neutron emission threshold $\langle\sigma_\nu^{\rm NC}\rangle$ have been calculated with $\langle E_\nu\rangle\approx 25$ MeV and $\eta_\nu\approx 0$. The corresponding interaction rates $\lambda_\nu^{\rm NC}$ are summed over four heavy-flavor neutrino species, and evaluated at $r=100$ km for a luminosity of 10^{51} erg s^{-1} per neutrino species. The last seven columns give $\langle n\rangle$, the average number of neutrons emitted after a neutral-current neutrino interaction, and various probabilities for multiple neutron emission.

Z	N	A	$\langle\sigma_\nu^{\rm NC}\rangle/A$ (10^{-42} cm^2)	$\lambda_\nu^{\rm NC}$ (s^{-1})	$\langle n\rangle$	$P_{n=1}$	$P_{n=2}$	$P_{n=3}$	$P_{n=4}$	$P_{n=5}$	$P_{n=6}$
28	50	78	0.56	3.5	2.0	0.45	0.26	0.16	0.11	0.02	0
48	82	130	0.94	9.7	2.0	0.37	0.40	0.14	0.08	0.01	0
68	126	194	0.75	11.6	2.0	0.41	0.37	0.10	0.08	0.03	0.01

than found experimentally, predicting concentrations of strength at both 7 and 17 MeV. This suggested to us that our somewhat restricted shell-model basis might not include enough of the correlations responsible for the GT resonance shape. (This conclusion has been confirmed by recent shell-model Monte Carlo calculations performed in the full $2p1f$ shell, which can describe reasonably well the measured GT-strength distributions in Fe and Ni nuclei [20].) Therefore we concluded that the value of Γ from (p,n) systematics, 5 MeV, is likely the more reliable choice.

Somewhat more sophisticated shell-model calculations were performed for the allowed neutral-current cross section. The ^{78}Ni ground state was calculated in the $1f2p1g_{9/2}$ model space, allowing all configurations with 0, 1, or 2 holes in the $1f_{7/2}$ shell. The distribution of $|M_{\rm GT}^{\rm NC}|^2$ was again evaluated by a method of moments, including configurations with three holes in the $1f_{7/2}$ shell and one particle in the $1g_{7/2}$ shell. That is, a complete basis was used for the final states. The resulting sum rule strength for $|M_{\rm GT}^{\rm NC}|^2$ was 6.35, yielding a quite large allowed cross section. But the strength was concentrated very near the ground state: 66.7% was within 3 MeV, 80% within 4 MeV, and 90% within 6 MeV, which the mass formula of Ref. [15] indicates is the neutron separation energy. Thus almost all of the strength is carried by bound states; the allowed contribution to neutron spallation, the process of present interest, is quite small, comparable to the forbidden contribution discussed below. This supports the assumptions that led to Eq. (10).

We were able to extend the tests of neutral-current cross sections to representative nuclei in each of the three r-process abundance peaks by performing CRPA calculations [21]. A Landau-Migdal interaction was used and all multipoles of both parities through $J=2$ were retained, thereby accounting for all allowed, first-forbidden and second-forbidden operators. Thus the CRPA calculations provide a check on the simpler Goldhaber-Teller treatment of first-forbidden neutrino scattering [16,18] and a cross-check on the shell-model result for the fraction of allowed strength in the continuum. The results for three representative nuclei are listed in Table II. They confirm the simple scaling estimate in Eq. (10) to within $\sim 40\%$. Within this accuracy, the results are independent of some of the existing neutrino spectrum uncertainties, such as whether $\eta_\nu\sim 3$ is more appropriate than $\eta_\nu\sim 0$. The average number of neutrons emitted $\langle n\rangle$ and the probabilities for multiple neutron emission, which are also listed in Table II, were obtained by folding the neutrino-induced excitation spectrum calculated in the CRPA with the neutron-evaporation spectrum determined from the statistical model [14]. We find that GT transitions contribute about 40% to the continuum cross sections, in agreement with the shell-model result for ^{78}Ni. Their contribution to $\langle n\rangle$ is, however, less than 30% due to the lower excitation energies characterizing the allowed transitions.

III. NEUTRINO-NUCLEUS INTERACTIONS DURING THE *R* PROCESS

The dynamic phase of the r process is thought to occur between temperatures of $\sim 3\times 10^9$ and $\sim 10^9$ K, during which time $(n,\gamma)\rightleftharpoons(\gamma,n)$ equilibrium is maintained. As photodisintegration reactions are typically orders of magnitude faster than competing neutral-current neutrino spallation reactions, it is clear that inelastic neutrino scattering has no effect in the dynamic phase. In contrast, charged-current neutrino reactions affect the charge flow and thus compete with β decay, particularly near the waiting points where β-decay rates are anomalously small. These charged-current effects will be discussed in this section. Below $\sim 10^9$ K the material freezes out from $(n,\gamma)\rightleftharpoons(\gamma,n)$ equilibrium, fixing the distribution of the r-process progenitor nuclei, which decay back to the valley of β stability to produce the abundances observed in nature. After the freeze out, neutrino interactions can affect the abundance distribution, with both charged-current reactions and heavy-flavor neutral-current scattering being important. We will discuss several interesting consequences of this neutrino postprocessing in Sec. IV.

Type-II supernovas have long been discussed as a possible site of the r process. As mentioned in the introduction, in the recently developed r-process model of Woosley *et al.* [2] the synthesis occurs in the ''hot bubble'' expanding off the neutron star, with the freeze out from $(n,\gamma)\rightleftharpoons(\gamma,n)$ equilibrium occurring at radii of 600–1000 km and at times ~ 10 s after core bounce. However, despite the appeal of the hot bubble as an r-process site, there are aspects of this model that are unsatisfactory, such as overproduction of the isotopes ^{88}Sr, ^{89}Y, and ^{90}Zr and the need for very high entropies. For this reason we will avoid the choice of a specific r-process model, instead exploring a more general scenario motivated by recent studies of nucleosynthesis in a neutrino-driven wind blown off the neutron star [22]. Such a wind can be described as an expanding bubble where the material temperature decreases as $T\propto 1/r$ and the outflow velocity increases as $v\propto r$ under the following assumptions: (1) the mass outflow rate is constant; (2) the expansion of the

radiation-dominated material in the outflow is adiabatic; and (3) the outflow is (barely) successful in ejecting mass to infinity. The time evolution for the radius of an expanding mass element in the outflow is given by

$$r(t) \propto \exp(t/\tau_{\rm dyn}), \tag{11}$$

where $\tau_{\rm dyn}$ is a characteristic dynamic time scale for the expansion. We will denote the radius and neutrino luminosity for a mass element at freeze out, $T \sim 10^9$ K, by $r_{\rm FO}$ and $L_{\nu,{\rm FO}}$, respectively. We assume that the individual neutrino luminosities are the same and generically denote L_ν as the luminosity for any neutrino species. The protoneutron-star neutrino luminosity is assumed to evolve with time as $\exp(-t/\tau_\nu)$, with $\tau_\nu \sim 3$ s.

In keeping with the notion that the discussion should be as general as possible, we will treat $\tau_{\rm dyn}$, $r_{\rm FO}$, and $L_{\nu,{\rm FO}}$ as parameters relevant to the freeze out of a particular peak. That is, their values for the $A \sim 80$ ($N=50$) peak could be different from those for the $A \sim 130$ or 195 ($N=82$ or 126) peak. This may be a prudent generalization given the ongoing debate [23] over whether r-process abundances are consistent with a single production site. Furthermore, even if there is only one r-process site, because the neutron-to-seed ratio required to produce each peak is different, individual peaks likely have to be made at different times, and hence under different conditions in a single site.

We first repeat the argument of Fuller and Meyer [6], who placed a lower bound on the freeze-out radius by demanding that the r process must be in approximate steady-state local β-flow equilibrium at the time of freeze out, a condition that Kratz *et al.* [5] deduced from the proportionality between the progenitor abundances along closed-neutron shells and the corresponding β-decay lifetimes. In local equilibrium, the product $\lambda(Z,N)Y(Z,N)$, where λ is the total charge-increasing rate and Y the abundance, should be independent of (Z,N). The rate λ includes both β decay and neutrino reactions, and if the latter are made too strong, the observed local equilibrium that holds when only β decay is considered is then destroyed. Using the reaction rates in Table I, the condition that local β-flow equilibrium holds to within 20% at freeze out is especially restrictive at $N=50$, yielding

$$\left(\frac{L_{\nu,{\rm FO}}}{10^{51}\ {\rm erg\ s^{-1}}}\right)\left(\frac{100\ {\rm km}}{r_{\rm FO}}\right)^2 \lesssim 0.12 \quad {\rm for}\ A \sim 80, \tag{12}$$

where this result corresponds to Fig. 2(a) of Ref. [6] [the comparison of $(Z,N)=(29,50)$ and $(30,50)$, which generated the most stringent limit] and depends on the β-decay rates in Table 4 of that reference. Equation (12) is sufficient to guarantee that local β-flow equilibrium holds at freeze out provided that $\tau_{\rm dyn}$ is longer than but still comparable to typical β-decay lifetimes, which are ~ 0.5 s at $N=50$. For the conditions in the r-process model of Woosley *et al.* [2], $L_{\nu,{\rm FO}} \sim 10^{51}$ erg s^{-1} and $r_{\rm FO} \sim 600$–1000 km, Eq. (12) is easily satisfied. But it is clear that freeze-out radii of ~ 300 km are also compatible with this constraint. If the calculation is repeated for the $N=82$ and 126 peaks [corresponding to $(Z,N)=(45,82)$ and $(46,82)$, and to $(67,126)$ and $(68,126)$, respectively, which we found generated the most stringent limits], the right-hand side of Eq. (12) becomes 0.83 and 0.37, respectively. We have used the β-decay rates calculated by Möller *et al.* [24] for the $N=126$ nuclei. The numerical values for the right-hand side of Eq. (12) may change somewhat if, for example, different ν_e energy spectra (see Ref. [6]) are used to calculate the rates in Table I.

We now examine the effects of charged-current reactions prior to freeze out for the generic neutrino-driven wind r-process model in order to assess whether neutrino interactions can speed up the charge flow past waiting-point nuclei, given the constraint imposed by Eq. (12). The results in Table I show that charged-current reaction rates in the waiting-point regions of $N=50$, 82, and 126 are reasonably constant, with $\overline{\lambda}_\nu^{\rm CC} = [(1/n)\Sigma_{i=1}^n 1/\lambda_i]^{-1} \approx 5.2$, 5.7, and 8.5 s^{-1}, respectively, being average values at $r=100$ km when $L_\nu = 10^{51}$ erg s^{-1}. The number of transitions (charge increase) ΔZ_ν induced by the neutrino irradiation is then

$$\Delta Z_\nu = \int_{t_i}^{t_f} \overline{\lambda}_\nu^{\rm CC}\left[\frac{L_\nu(t)}{10^{51}\ {\rm erg\ s^{-1}}}\right]\left[\frac{100\ {\rm km}}{r(t)}\right]^2 dt, \tag{13}$$

where t_i and t_f are the initial and final times, respectively, corresponding to the r-process epoch between 3×10^9 and 10^9 K. Under the generic wind scenario, this can be evaluated to give

$$\begin{aligned}\Delta Z_\nu &= \frac{9}{2}\,\overline{\lambda}_\nu^{\rm CC}\tau_{\rm dyn}\left(\frac{L_{\nu,{\rm FO}}}{10^{51}\ {\rm erg\ s^{-1}}}\right) \\ &\quad\times\left(\frac{100\ {\rm km}}{r_{\rm FO}}\right)^2 \frac{\exp[(\ln 3)\,\tau_{\rm dyn}/\tau_\nu] - 1/9}{1+\tau_{\rm dyn}/(2\tau_\nu)} \\ &\lesssim 0.54\overline{\lambda}_\nu^{\rm CC}\tau_{\rm dyn}\,\frac{\exp(1.1\tau_{\rm dyn}/\tau_\nu) - 1/9}{1+\tau_{\rm dyn}/(2\tau_\nu)} \quad {\rm for}\ A \sim 80,\end{aligned} \tag{14}$$

where the last line follows from the $N=50$ freeze-out condition of Eq. (12). Now this can be compared with the corresponding charge increase due to β decay,

$$\Delta Z_\beta = \overline{\lambda}_\beta(t_f - t_i) = (\ln 3)\overline{\lambda}_\beta\tau_{\rm dyn} \sim 1.1\overline{\lambda}_\beta\tau_{\rm dyn}, \tag{15}$$

where $\overline{\lambda}_\beta \sim 1.9$ s^{-1} at $N=50$, with the rates in Table 4 of Ref. [6]. Thus

$$\frac{\Delta Z_\nu}{\Delta Z_\beta} \lesssim 0.49\,\frac{\overline{\lambda}_\nu^{\rm CC}}{\overline{\lambda}_\beta}\,\frac{\exp(1.1\tau_{\rm dyn}/\tau_\nu) - 1/9}{1+\tau_{\rm dyn}/(2\tau_\nu)} \quad {\rm for}\ A \sim 80. \tag{16}$$

This result is quite interesting. It suggests that one can achieve an r-process freeze-out pattern with characteristic local β-flow equilibrium for the $N=50$ waiting-point nuclei while still having important—even dominant—neutrino contributions to the overall r-process charge flow. The above ratio is $\lesssim 1.2$ under the assumption $\tau_{\rm dyn} \ll \tau_\nu$. If $\tau_{\rm dyn} \sim \tau_\nu$, this ratio increases by a factor of ~ 2. If we repeat the calculation for $N=82$ (126), the numerical coefficient 0.49 on the right-hand side of Eq. (16) becomes 3.4 (1.5) so that, with $\overline{\lambda}_\beta \sim 4.3$ (16.0) s^{-1} at $N=82$ (126), $\Delta Z_\nu/\Delta Z_\beta \lesssim 4.0$ (0.71) when $\tau_{\rm dyn} \ll \tau_\nu$. Thus the charge flow can be totally dominated by charged-current neutrino interactions in the

$N=82$ peak without perturbing the local β-flow equilibrium at freeze out by more than 20%.

The possible importance of this is clear. The transit of the $N=50$ ''bottle neck'' requires a charge increase of $\Delta Z\sim 5$ and thus, if the flow is carried only by β decay, $\tau_{\rm dyn}$ must exceed 2.4 s, according to Eq. (15). This time is uncomfortably long for most neutrino-driven wind scenarios, where natural dynamic time scales are ~ 0.1–1 s [22]. Of course, one may resort to a scenario where the nuclear flow through the $N=50$ region is carried by α-capture reactions as in the r-process model of Woosley *et al.* [2] to accommodate such short time scales. However, even if the charge flow is only carried by weak interactions, the inclusion of charged-current neutrino reactions can reduce the time required to clear the $N=50$ bottle neck by more than a factor of two without destroying the β-flow equilibrium ''footprint'' characterizing the freeze out. Similarly, the very large charge flow enhancements possible in the $N=82$ peak allow, in principle, $\tau_{\rm dyn}$ as low as ~ 0.2 s. As most of the time required to make the $N=126$ peak is spent at the $N=82$ and possibly also the $N=50$ waiting-point nuclei, the required time scale for the r process to proceed through to completion is correspondingly shortened. Given conceivable uncertainties in the nuclear structure and in the ''memory'' of neutrino irradiation prior to freeze out, a $\tau_{\rm dyn}$ of ~ 0.1 s probably represents a lower bound on the time scale for the r process. Consistent with all of the arguments above, we shall entertain the possibility of $\tau_{\rm dyn}$ as low as ~ 0.1 s in the remainder of this paper.

There are yet other attractive aspects of intense neutrino irradiation during the r process: Fuller and Meyer [6] pointed out that charged-current reactions could help to correct the overproduction of nuclei near $N=50$ in the r-process scenario of Woosley *et al.* [2] by increasing the electron fraction mainly through ν_e capture on free neutrons. Furthermore, they showed that some interesting light p-process nuclei could be produced after including charged-current neutrino reactions on nuclei in the reaction network. Finally, McLaughlin and Fuller [7] pointed out that a substantial neutrino flux at the freeze out of the $N=82$ peak may improve the fit of the inferred progenitor abundances to the steady-state weak (β decay plus ν_e capture) flow equilibrium. Because the relative importance of ν_e-induced and β-decay-induced charge flow evolves during the r process, we may have reached a point where the explicit incorporation of such effects into reaction network simulations of the r process is needed. This may be essential to understanding the observed pattern of abundances.

IV. NEUTRINO POSTPROCESSING EFFECTS

As the temperature decreases to $\sim 10^9$ K, the material freezes out from $(n,\gamma)\rightleftharpoons(\gamma,n)$ equilibrium, leaving a distribution of r-process progenitor nuclei which, after decay back to the valley of β stability, produce the abundance patterns seen in nature.

The charged-current reactions discussed in the previous section can continue to influence the r-process abundance pattern during postprocessing by altering the (Z,N) path which the progenitors follow as they β decay. The process of interest, neutron emission following (ν_e,e^-) reactions, is superficially analogous to the β-delayed neutron emission process that is conventionally included in r-process calculations. However, the excitation energy of the daughter nucleus is significantly higher for neutrino reactions, leading to much higher probabilities of multiple neutron emission, as can be seen in Table I. Thus the inclusion of charged-current reactions in the postprocessing phase has the potential to push abundance peaks to significantly smaller A.

Furthermore, since the postprocessing phase is defined by the condition that $(n,\gamma)\rightleftharpoons(\gamma,n)$ equilibrium has broken down, the effects of neutral-current neutrino reactions are no longer competing with those of (γ,n) reactions. Nuclear excitation by (ν,ν') reactions above the particle breakup threshold may produce one or more neutrons, again shifting abundances to lower A. The important species, due to their higher mean energies, are the heavy-flavor neutrinos.

The optimal procedure for evaluating these neutrino irradiation effects would be to incorporate them directly into the network codes that follow the progenitors as they β decay. Our procedures here are less sophisticated, though we would argue that they are at least adequate qualitatively, given the other uncertainties in r-process calculations. We make three simplifications. First, as is apparent from Tables I and II, neutrino rates and neutron spallation yields do not vary excessively over an abundance peak. For example, in the $N=50$ peak, $\lambda_\nu^{\rm CC}$ varies by about $\pm 40\%$, while the average number of neutrons emitted per neutrino event $\langle n\rangle$ varies by about $\pm 30\%$. (Variations between peaks are more significant: $\langle n\rangle$ for $N=126$ is about twice that for $N=50$.) Thus it is a reasonable approximation to extract from Table I average values $\overline{\lambda_\nu^{\rm CC}}$, as we did in Sec. III, as well as averages for the probabilities of emitting n neutrons following a neutrino interaction $\overline{P_n^{\rm CC}}$. Similarly, we take the values in Table II as representative of the entire peaks near $N=50$, 82, and 126. Second, we make the additional simplification that these mean progenitor rates and neutron emission probabilities can be used throughout the postprocessing phase, even as $N-Z$ is evolving due to β decay and charged-current neutrino reactions. This is probably a quite good assumption for neutral-current reactions because rates are tied to the TRK sum rule and neutron emission probabilities to the location of the giant resonances, both of which are only weakly dependent on $N-Z$ for not too large changes in A. It is a more dangerous approximation in the case of charged-current reactions because the available allowed strength and $\langle n\rangle$ are strongly correlated with $N-Z$. Therefore, results for cases where $\tau_{\rm dyn}$ is long compared with typical β decay and/or ν_e capture lifetimes should be viewed with caution. Third, we do not consider the subsequent processing of neutrons liberated in the spallation. The neutron reabsorption process is quite different from the neutrino-induced multiple-neutron spallation process, as only one neutron is captured at a time. In addition, the reabsorption should take place over the broad range of nuclei with reasonable abundances and strong (n,γ) cross sections that reside below the abundance peaks, as well as on the more plentiful nuclei with smaller, but not unimportant neutron capture cross sections that lie on the high-mass side of the abundance peaks. This contrasts with the neutrino-induced neutron spallation reactions, where dramatic effects occur only for 3 or 5 nuclei concentrated in

TABLE III. Postprocessing neutron emission probabilities in the $A\sim130$ region. The fluence $\mathcal{F}$ is defined in Eq. (18). The second column gives $\langle n\rangle$, the average number of neutrons emitted by a nucleus throughout the postprocessing, e.g., allowing for the possibility of multiple neutrino interactions. Both charged-current and neutral-current interactions are included.

$\mathcal{F}$	$\langle n\rangle$	$P_{n=0}$	$P_{n=1}$	$P_{n=2}$	$P_{n=3}$	$P_{n=4}$	$P_{n=5}$	$P_{n=6}$	$P_{n=7}$	$P_{n=8}$	$P_{n=9}$	$P_{n\geq10}$
0.010	0.339	0.857	0.031	0.053	0.043	0.010	0.003	0.002	0.001	0	0	0
0.015	0.508	0.794	0.043	0.073	0.061	0.017	0.007	0.003	0.001	0	0	0
0.020	0.677	0.735	0.053	0.091	0.077	0.023	0.011	0.006	0.002	0.001	0	0
0.030	1.016	0.630	0.069	0.119	0.103	0.037	0.021	0.012	0.005	0.002	0.001	0.001
0.040	1.355	0.540	0.078	0.137	0.123	0.051	0.033	0.020	0.009	0.005	0.002	0.002
0.050	1.693	0.463	0.084	0.148	0.137	0.063	0.045	0.029	0.015	0.008	0.004	0.004
0.060	2.032	0.397	0.086	0.154	0.146	0.075	0.056	0.038	0.021	0.012	0.007	0.008

special ''windows.'' Therefore, while there may be consequences associated with neutron recapture, we expect its net effect will be global and gentle, thus not undoing the neutrino postprocessing effects described below.

With these approximations, the neutrino postprocessing effects can be evaluated without reference to the details of the r process. This is helpful in illustrating the kinds of effects that might result from the neutrino irradiation. The starting point is to calculate the mean number of neutrino events $N(n)$ producing exactly n neutrons in the subsequent spallation by integrating over all times after freeze out,

$$\begin{aligned}\overline{N(n)}&=(\overline{P_n^{\mathrm{NC}}}\overline{\lambda_\nu^{NC}}+\overline{P_n^{\mathrm{CC}}}\overline{\lambda_\nu^{\mathrm{CC}}})\left(\frac{L_{\nu,\mathrm{FO}}}{10^{51}\ \mathrm{erg\ s^{-1}}}\right)\\&\quad\times\left(\frac{100\ \mathrm{km}}{r_{\mathrm{FO}}}\right)^2\int_0^\infty\exp\left[-t\left(\frac{2}{\tau_{\mathrm{dyn}}}+\frac{1}{\tau_\nu}\right)\right]dt\\&=(\overline{P_n^{\mathrm{NC}}}\overline{\lambda_\nu^{\mathrm{NC}}}+\overline{P_n^{\mathrm{CC}}}\overline{\lambda_\nu^{\mathrm{CC}}})\left(\frac{L_{\nu,\mathrm{FO}}}{10^{51}\ \mathrm{erg\ s^{-1}}}\right)\\&\quad\times\left(\frac{100\ \mathrm{km}}{r_{\mathrm{FO}}}\right)^2\frac{\tau_{\mathrm{dyn}}/2}{1+\tau_{\mathrm{dyn}}/(2\tau_\nu)}.\end{aligned}\tag{17}$$

Comparing the rates in Tables I and II, we see that $\overline{\lambda_\nu^{\mathrm{NC}}}$ is about 1.7 and 1.4 times $\overline{\lambda_\nu^{\mathrm{CC}}}$ for the $N=82$ and 126 peaks, respectively. But the average number of neutrons emitted per charged-current interaction is about twice that for neutral-current interactions in the $N=126$ peak, a consequence of the large neutron excess and subsequent high excitation energy of the daughter nucleus following (ν_e,e^-) interactions. Thus charged-current and neutral-current interactions are of comparable importance in driving neutron spallation near $N=126$.

Now in a neutrino-driven wind governed by τ_{dyn} and τ_ν, a given nucleus can interact one or more times, emitting several neutrons. We would like to calculate the net probability that, at the end of postprocessing, a given progenitor nucleus has lost n neutrons. The assumptions we have enumerated above make this a straightforward exercise: rates and neutron emission probabilities are not affected by the prior history of the target nucleus. Thus the distribution of events of each type—e.g., the distribution of neutrino events that produce exactly n spallation neutrons—is governed by a Poisson distribution with parameter $\overline{N(n)}$. The overall probability for emitting some number of neutrons is given by counting up the number of ways this can be done (e.g., two neutrons can be ejected by one neutrino interaction that knocks out two, or by two interactions each of which knocks out one), and folding the Poisson probabilities for each type of events in the product. The resulting distributions, which are not Poissonian, are tabulated in Tables III and IV for the $N=82$ and 126 peaks, respectively, and depend on the dimensionless parameter

$$\begin{aligned}\mathcal{F}&=\int_{t_f}^\infty\left[\frac{L_\nu(t)}{10^{51}\ \mathrm{erg\ s^{-1}}}\right]\left[\frac{100\ \mathrm{km}}{r(t)}\right]^2dt\\&=\frac{1}{2}\left(\frac{L_{\nu,\mathrm{FO}}}{10^{51}\ \mathrm{erg\ s^{-1}}}\right)\left(\frac{100\ \mathrm{km}}{r_{\mathrm{FO}}}\right)^2\left(\frac{\tau_{\mathrm{dyn}}}{\mathrm{s}}\right)\frac{1}{1+\tau_{\mathrm{dyn}}/(2\tau_\nu)},\end{aligned}\tag{18}$$

which is the neutrino fluence in units of 10^{47} erg km^{-2}. In

TABLE IV. As in Table III, but for the $A\sim195$ region.

$\mathcal{F}$	$\langle n\rangle$	$P_{n=0}$	$P_{n=1}$	$P_{n=2}$	$P_{n=3}$	$P_{n=4}$	$P_{n=5}$	$P_{n=6}$	$P_{n=7}$	$P_{n=8}$	$P_{n=9}$	$P_{n\geq10}$
0.010	0.609	0.818	0.039	0.036	0.013	0.043	0.036	0.007	0.002	0.002	0.002	0.002
0.015	0.914	0.740	0.053	0.050	0.019	0.059	0.051	0.012	0.005	0.004	0.004	0.003
0.020	1.218	0.669	0.064	0.061	0.024	0.073	0.064	0.017	0.008	0.006	0.007	0.007
0.030	1.827	0.547	0.078	0.076	0.033	0.092	0.084	0.029	0.016	0.013	0.013	0.019
0.040	2.436	0.448	0.086	0.085	0.040	0.104	0.097	0.041	0.024	0.020	0.021	0.034
0.050	3.045	0.366	0.087	0.089	0.045	0.110	0.106	0.051	0.033	0.028	0.029	0.056
0.060	3.654	0.300	0.086	0.090	0.048	0.112	0.111	0.060	0.041	0.035	0.036	0.081

the supernova r-process model of Woosley *et al.* [2], freeze out occurs at radii of 600–1000 km over a dynamic time scale of $\tau_{\rm dyn}\sim\tau_\nu\sim 3$ s. In this case, $\mathcal{F}$ would lie in the range ~ 0.01–0.03. Thus, for such long $\tau_{\rm dyn}$, appreciable neutrino postprocessing can occur even at such large freeze-out radii, as is apparent from Tables III and IV (and from the discussion below).

It is obvious from Eq. (18) that postprocessing effects have an explicit and sensitive dependence on $\tau_{\rm dyn}$, especially for $\tau_{\rm dyn}<\tau_\nu$. This was not the case for the neutrino effects that occur prior to the freeze out: the condition of local β-flow equilibrium at freeze out [Eq. (12)] constrains the neutrino luminosity and radius, or equivalently the neutrino flux at freeze out. As mentioned previously, local β equilibrium can be obtained under this condition as long as $\tau_{\rm dyn}$ is longer than, but still comparable to the typical β-decay lifetimes for the relevant abundance peak. Likewise, the fractional increase in r-process charge flow due to neutrinos [Eq. (16)] has a significant dependence on $\tau_{\rm dyn}$ only for long dynamic time scales $\tau_{\rm dyn}\sim\tau_\nu$. We can set a lower limit on $\tau_{\rm dyn}$ by requiring a minimum charge increase in making the abundance peak only when Eqs. (12), (15), and (16) are combined together. On the other hand, Eq. (18) shows that considerations of neutrino postprocessing effects can provide important information about $\tau_{\rm dyn}$ and the neutrino flux at freeze out independent of the details of the r process.

The proper use of the results in Tables III and IV is a nontrivial issue. Neither our prejudices about $\tau_{\rm dyn}$ nor the freeze-out constraints similar to Eq. (12) significantly constrain the neutrino fluence $\mathcal{F}$ in Eq. (18). For a large fluence, a naive perturbative folding of a calculated r-process abundance distribution with these spallation probabilities could be misleading. Worse, the calculated initial distribution would have likely been ''tuned'' to reproduce observation, fitting, for example, the abundance peak at $N=82$. But tuning prior to postprocessing is clearly inappropriate: one should strive to produce a best fit only after the final postprocessed distribution is achieved.

There is an alternative strategy that is appealing in its simplicity and avoids the need for a ''base-line'' unpostprocessed distribution from theory: begin with the observed r-process abundance distribution and, for a given neutrino fluence, invert this distribution to derive the yields that must have existed prior to postprocessing. This distribution would be the one conventional theory should match, if indeed the neutrino postprocessing effects are as described here. Part of the appeal of this procedure is that the final r-process abundance distribution is rather tightly constrained by observation and the neutrino physics is relatively simple, governed by a single parameter $\mathcal{F}$ in the wind scenario. [In fact, Eq. (18) also gives the general definition of $\mathcal{F}$ in any supernova r-process model.] Thus we can derive the unpostprocessed distribution with some confidence. Note however, some caution must be exercised when one compares the unpostprocessed distribution derived this way with the progenitor abundance pattern at freeze out calculated in r-process models. This is because effects of β-delayed neutron emission on the freeze-out pattern are hard to deconvolve in general, although neutrino postprocessing commutes with β-delayed neutron emission under the assumption of target-independent neutrino-induced neutron spallation.

In the region of an abundance peak, the inversion is relatively simple to carry out iteratively. As an initial guess for the unpostprocessed distribution, we take the solar r-process abundances. The postprocessing is calculated, and the deviations between the resulting distribution and observed abundances are then used to guess a new unpostprocessed distribution. The procedure is then iterated until the unpostprocessed distribution converges, i.e., yields a postprocessed distribution in agreement with observation. Depending on the neutrino fluence, the final abundance of a particular nucleus is affected by only a specific number of nuclei with higher masses. Therefore, one can use an alternative inversion procedure by only considering possible postprocessing contributions from nuclei below a cutoff high mass nucleus sufficiently far away from the peak, say 10 mass units above the peak nucleus. Starting from the cutoff nucleus, one can calculate the unpostprocessed abundances of nuclei with successively lower masses. These two procedures yield the same results except near the cutoff high mass nucleus. In other words, our postprocessing results are insensitive to the choice of the cutoff, so long as it is sufficiently far away from the peak.

A. The $N=82$ peak

The first result one can get from such an analysis is an upper bound on the neutrino fluence $\mathcal{F}$ in Eq. (18). The region of greatest sensitivity to the postprocessing are those isotopes of low abundance lying just below the $N=82$ peak: the inversion shows that the region $A=124$–126 is particularly sensitive to the neutrino irradiation. The requirement that these isotopes not be overproduced provides a stringent constraint on the neutrino fluence: if the parameter $\mathcal{F}$ in Eq. (18) is made too large, the inversion gives unphysical (negative) unpostprocessed abundances for these nuclei.

The deduced limit on the parameter of Eq. (18)

$$\mathcal{F}=\frac{1}{2}\left(\frac{L_{\nu,\rm FO}}{10^{51}\ \rm erg\ s^{-1}}\right)\left(\frac{100\ \rm km}{r_{\rm FO}}\right)^2\left(\frac{\tau_{\rm dyn}}{\rm s}\right)\frac{1}{1+\tau_{\rm dyn}/(2\tau_\nu)}$$
$$\lesssim 0.045\ \ \text{for}\ \ A\sim 130 \tag{19}$$

is quite stringent. For such a fluence, the neutrino postprocessing contributions to the abundances of ^{124}Te, ^{125}Te, and ^{126}Te are 0.24, 0.45, and 0.65, respectively, which can be compared with the corresponding ranges deduced from observation, 0.215 ± 0.020, 0.269 ± 0.042, and 0.518 ± 0.126 [25]. Thus this fluence is sufficient to overproduce all three isotopes, with the ^{125}Te discrepancy being particularly severe (4σ).

This limit, when combined with the freeze-out constraints we derived following Fuller and Meyer [6], defines an allowed region of neutrino fluxes at freeze-out and dynamic time scales, as shown in Fig. 1(a). In this figure, the horizontal solid line corresponds to the upper limit on the neutrino flux at freeze out similar to Eq. (12), but for the $A\sim 130$ $(N=82)$ peak. The diagonal solid line corresponds to the upper bound on the neutrino fluence after freeze out in Eq. (19) for the same peak. The region bounded by these two

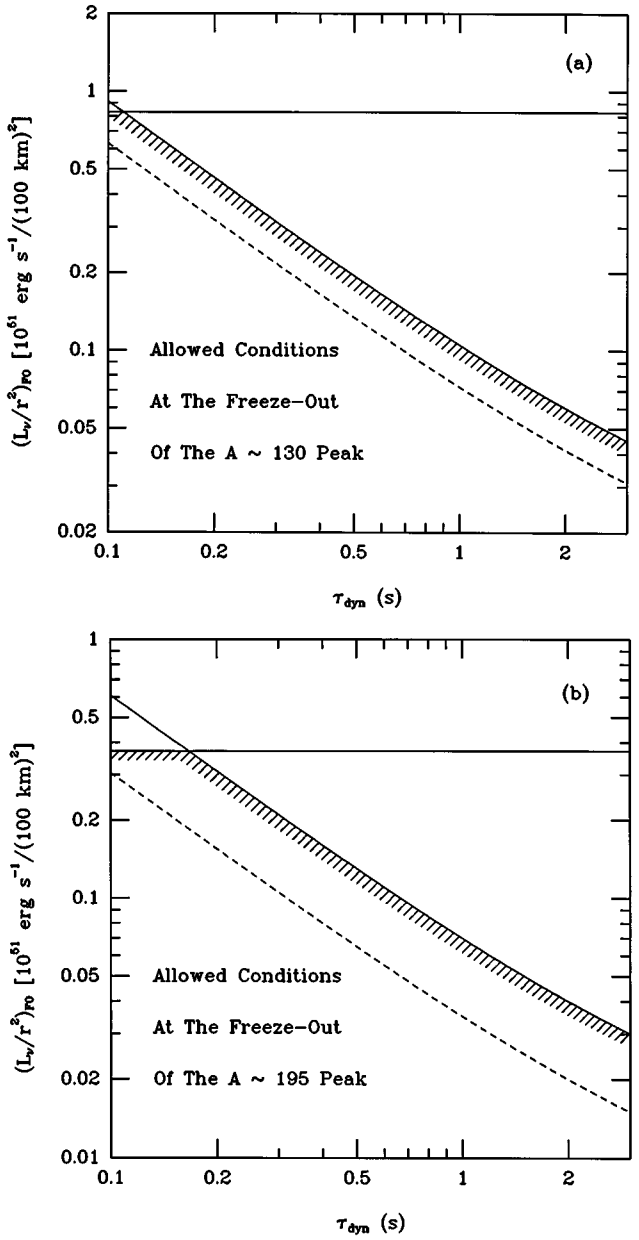

FIG. 1. Constraints imposed on the neutrino flux L_ν/r^2 at freeze out and dynamic time scale $\tau_{\rm dyn}$ by the conditions (horizontal solid lines) of local β-flow equilibrium at the freeze out of (a) the $A\sim 130$ peak, and (b) the $A\sim 195$ peak, and by the conditions (diagonal solid lines) that neutrino postprocessing not overproduce nuclei in the regions of (a) $A=124$–126, and (b) $A=183$–187. We have taken $\tau_\nu=3$ s. Parameters lying on the dashed lines correspond to the fluences determined by attributing the synthesis of nuclei in the special mass regions to neutrino postprocessing only (see text). Note that the allowed parameter regions can be reduced if further requirements of the r-process are imposed.

lines gives the allowed conditions at the freeze out of the $A\sim 130$ peak.

As the neutrino postprocessing calculations point to the $A=124$–126 region as being most sensitive to such effects, it is interesting to examine this region more carefully. Using a fluence of $\mathcal{F}=0.031$, which is compatible with Eq. (19), one finds abundances of 0.18, 0.35, and 0.50 for $A=124$, 125, and 126, respectively. As the agreement with the observed abundances given in the paragraph above is quite good, the comparison hints that this region might be one where neutrino postprocessing effects dominate the production. This would, of course, be an exciting result as any determination of the postprocessing fluence would quantitatively constrain the location and dynamic time scale for the r process, through an equality analogous to Eq. (19). In this connection, we note that standard (unpostprocessed) r-process calculations often significantly underestimate abundances in a relatively broad region around $A\sim 120$ (see Kratz *et al.* in Ref. [1]), so there is room for additional production. (As large postprocessing effects are confined to the region $A=124$–126, they are not a solution for all of the deficiencies in the $A\sim 120$ region. Effects such as shell quenching, which would revise the mass formulas commonly used, also help to reduce the discrepancies [26].)

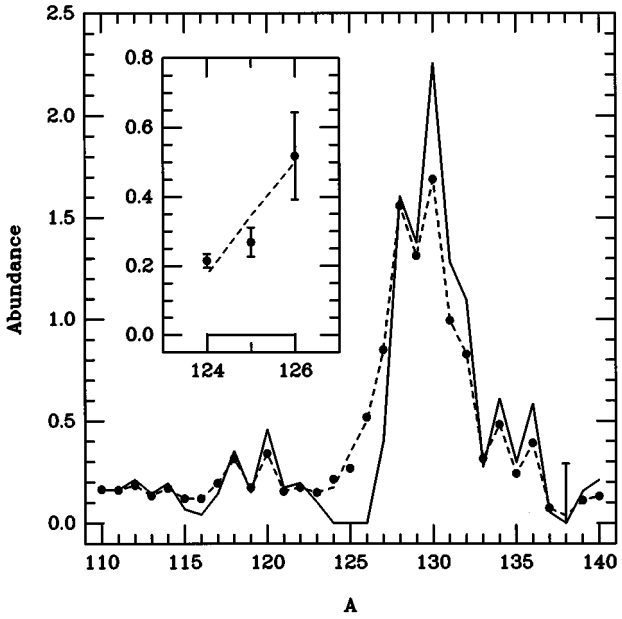

FIG. 2. The unpostprocessed distribution (solid line) obtained from the observed r-process abundances of Ref. [25] by unfolding the neutrino postprocessing effects. We have chosen a fluence [Eq. (18)] of $\mathcal{F}=0.031$, which provides a best fit to the observed abundances of the nuclei with $A=124$–126 as highlighted in the inset. The filled circles and error bars are data taken from Ref. [25]. The dashed line essentially going through all the filled circles corresponds to the postprocessed distribution.

We performed the inversion under the assumption that the nuclei in the $A=124$–126 window are attributable entirely to the postprocessing, that is, for a fluence [Eq. (18)] of $\mathcal{F}=0.031$. The solid line in Fig. 2 is the resulting unpostprocessed distribution. The r-process abundance distribution deduced from solar abundances is also shown in this figure as filled circles. The dashed line essentially going through all the filled circles is the abundance pattern that results from the neutrino postprocessing of the solid curve. To highlight the neutrino-induced synthesis of the nuclei in the $A=124$–126 window, we blow up this region in the inset of Fig. 2, and plot the error bars on the observed solar r-process abundances. As we can see, all three nuclei are produced within $\sim 1\sigma$ of the observed abundances for a single neutrino fluence.

There are a few additional features clear from Fig. 2:

(1) The fluence of $\mathcal{F}=0.031$ corresponds to an average neutron emission number of $\langle n\rangle=1.05$. Thus one might expect to see a shift in the peak of the distribution by this much. This does not occur because most nuclei (62%) do not interact with the neutrino flux: an $\langle n\rangle$ of 1.05 is achieved largely through the emission of two or three neutrons by $\sim 20\%$ of the nuclei.

(2) Therefore, the signature of neutrino postprocessing is not a shift in the peak, but rather a distortion of the shape of the peak. Features tend to be more exaggerated before postprocessing: The $A\sim 130$ peak is higher before postprocessing, its edge on the low-mass side is steeper, and the valley at $A=124$–126 is deeper. Thus the net effect of the postprocessing on the lower two-thirds of the abundance peak is not unlike that of pressing on a steep pile of sand.

(3) In addition to spreading the abundance peak, the postprocessing has a modest smoothing effect. If one calculates the average magnitude of the ratio of the difference between neighboring peaks and valleys to half their sum, it is 1.00 before postprocessing and 0.61 after. These averages were evaluated in the region between masses 114 and 136.

B. The $N=126$ peak

The analogous inversion in the region of the $N=126$ abundance peak again revealed a region on the low-mass tail of the peak where postprocessing contributions are especially pronounced. This region spans the mass numbers $A=183$–187 and thus the nuclei ^{183}W, ^{184}W, ^{185}Re, ^{186}W, and ^{187}Re. As in the $N=82$ peak, we establish a conservative upper bound on the neutrino fluence by finding the inversion conditions under which all of these nuclei are overproduced by the postprocessing alone,

$$\mathcal{F}=\frac{1}{2}\left(\frac{L_{\nu,\mathrm{FO}}}{10^{51}\ \mathrm{erg\ s^{-1}}}\right)\left(\frac{100\ \mathrm{km}}{r_{\mathrm{FO}}}\right)^2\left(\frac{\tau_{\mathrm{dyn}}}{\mathrm{s}}\right)\frac{1}{1+\tau_{\mathrm{dyn}}/(2\tau_\nu)}$$
$$\lesssim 0.030\ \text{ for }\ A\sim 195. \tag{20}$$

A fluence saturating this bound overproduces all five species, with the deviations being $\gtrsim 3\sigma$ in four cases (and with the disagreement for ^{187}Re being particularly large, 0.067 compared with 0.0373 ± 0.0040 [27]). The constraint in Eq. (20) can be combined with the freeze-out bound of Sec. III again to severely limit the allowed neutrino flux at freeze out and the dynamic time scale. The results are given in Fig. 1(b).

The appearance of a well-defined region where neutrino postprocessing effects are particularly pronounced suggests again that we test the ansatz that these nuclei are entirely products of the postprocessing. For a fluence of $\mathcal{F}=0.015$, one obtains

$A=183$ 0.0053 0.0067 ± 0.0016 [27],

$A=184$ 0.0093 0.0135 ± 0.0035 [27],

$A=185$ 0.0160 0.0127 ± 0.0024 [27],

$A=186$ 0.0274 0.0281 ± 0.0024 [27],

$A=187$ 0.0411 0.0373 ± 0.0040 [27],

where the first number is the postprocessing result and the second the abundance deduced from observation. The correspondence is quite good and these results, especially when considered together with the $N=82$ results, are very suggestive.

We again stress that the regions where postprocessing effects are most important, $A=124$–126 and 183–187, are clearly identified by the inversion procedure, the input to which consists of the neutrino cross sections and the associated multiple neutron emission probabilities we have calculated and the r-process abundances derived from observation. The identification of these regions as sensitive to postprocessing does not, of course, require that the postprocessing effects be large. That will depend on where the r process occurs in the supernova—or whether the supernova is even the correct site. But as we can do the inversion for any assumed neutrino fluence, the pattern of abundances in these regions can either help to confirm or rule out the possibility of important neutrino-induced synthesis. We find that the observed abundance pattern in both regions is characteristic of neutrino postprocessing.

Provided we have not been misled by an unfortunate conspiracy of numbers, the conclusions would appear to be very important. First, this suggests that a core-collapse supernova (or at least some environment characterized by a similarly intense neutrino fluence) is the site of the r process. Second, the required fluences to produce the $A=124$–126 and 183–187 isotopes can be calculated and are $\mathcal{F}=0.031$ and 0.015, respectively. Thus we have been able to place an important constraint on the r process independent of the many uncertainties that usually enter into network simulations. As these fluences are modest, it appears either that the freeze outs occur at large radii or that the dynamic time scales are short. Most importantly, the derived postprocessing fluence sharply constrains any model of the supernova r-process nucleosynthesis. For example, in the neutrino-driven wind model discussed, τ_{dyn} is now determined as a function of the neutrino flux at freeze out, or the freeze-out radius given the neutrino luminosity. The third conclusion, which is more uncertain, is that the factor of two difference in the $N=82$ and 126 postprocessing fluences suggests that the $N=82$ peak freezes out at a smaller radius than the $N=126$ peak in a dynamic r-process model such as the neutrino-driven wind. In the wind models, large neutrino luminosities tend to drive faster expansions of the outflow, and hence correspond to shorter dynamic time scales [22]. As a result, the effects of τ_{dyn} and L_ν on the fluence $\mathcal{F}$ nearly cancel. Therefore, a larger fluence implies a smaller freeze-out radius. (The reason for being cautious with this conclusion is that the determination of the $N=82$ fluence depends on only three isotopes, so the possibility of an unfortunate neutron-capture mimicking of the $A=124$–126 postprocessed abundances is not out of the question. In addition, a consistent set of neutrino luminosity, dynamic time scale, and freeze-out radius corresponding to a specific fluence can only be obtained in a detailed model of the neutrino-driven wind.)

In Fig. 3 we present the results of the inversion—the r-process abundance distribution before neutrino postprocessing that would reproduce observation—for the $N=126$ peak and for a fluence of $\mathcal{F}=0.015$. The qualitative aspects of this distribution are quite similar to those found for the

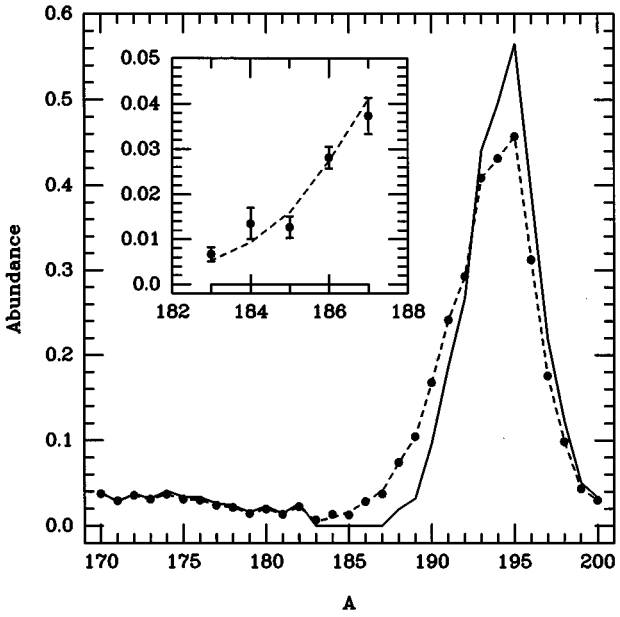

FIG. 3. As in Fig. 2, but for the $N=126$ region. A neutrino fluence [Eq. (18)] of $\mathcal{F}=0.015$ has been used, as required by the neutrino postprocessing fit to the $A=183$–187 region. Solar r-process abundances are taken from Ref. [25] except for the $A=182$–189 region, where the revised data of Ref. [27] have been used.

$N=82$ peak: the features of the distribution before postprocessing are more distinct. This fluence corresponds to an average neutron emission number of $\langle n\rangle=0.914$. But, as in the $N=82$ case, this is accomplished by a small fraction of the nuclei emitting multiple neutrons after neutrino interactions: 74% of the nuclei experience no interactions. Thus there is no shift in the peak of the abundance distribution.

V. CONCLUSIONS

In this paper we have explored the consequences of neutrino irradiation during both the dynamic $[(n,\gamma)\rightleftharpoons(\gamma,n)$ equilibrium] and postprocessing phases of the r process. Our calculations are based on reasonable treatments of both charged-current and neutral-current responses in the relevant nuclear mass regions, and include important contributions from forbidden transitions in the case of $\nu_{\mu(\tau)}$ and $\overline{\nu}_{\mu(\tau)}$ interactions.

Following Fuller and Meyer [6], we used the ν_e capture rates and the observation of approximate local β-flow equilibrium in the abundance peaks to constrain the radius (and neutrino luminosity) at freeze out. We then showed that this constraint still allows important—in fact, dominant in the case of the $N=82$ peak—neutrino contributions to the overall r-process charge flow. This is an interesting result since the times required to cross the $N=50$ and 82 peaks are, in the absence of neutrino effects, uncomfortably long.

We then studied the postprocessing phase. Because the neutrino effects are relatively well understood, we argue that the unpostprocessed abundance distribution can be reasonably well determined from observation as a function of the neutrino fluence. The result is the identification of two regions, $A=124$–126 and 183–187, that are particularly sensitive to neutrino postprocessing. Furthermore, the pattern of abundances in both regions corresponds closely to that from neutrino-induced neutron spallation. Thus there is strong evidence that these eight isotopes are mainly produced by neutrino postprocessing.

If this chain of argument is correct, the r process must take place in an intense neutrino fluence. This supports the growing prejudice for a site within a core-collapse supernova. The allowable dynamics of such supernova models are now sharply constrained by the deduced postprocessing fluence: for a given freeze-out radius and neutrino luminosity, the dynamic time scale is determined. A comparison of the fluences for the $N=82$ and 126 peaks also hints of a dynamic r process where the $N=82$ peak freezes out at a smaller radius.

Although the deduced fluences dominate the nucleosynthesis only in the special regions of $A=124$–126 and 183–187, their effects elsewhere are not insignificant. The features of the unpostprocessed distributions are significantly more pronounced than those of the final distributions. Thus if one is interested in supernova r-process sites with even modest neutrino irradiation, it is unwise to tune network simulations to reproduce final r-process abundance distributions unless the neutrino effects have been evaluated.

The present calculations involved several ''short cuts'' that, though reasonable, should be reexamined in future calculations. We believe our results provide ample motivation for a full inclusion of neutrino effects in r-process networks.

ACKNOWLEDGMENTS

We thank George Fuller, Brad Meyer, and Friedel Thielemann for helpful discussions, and especially thank George Fuller and Gail McLaughlin for comments that helped us in improving this paper. Y.-Z. Qian and P. Vogel acknowledge the Institute for Nuclear Theory at University of Washington, Seattle for its hospitality during the time part of this work was done. This work was supported by the Department of Energy under Grant Nos. DE-FG06-96ER40561 and DE-FG03-88ER-40397, and by the National Science Foundation under Grant Nos. PHY94-12818 and PHY94-20470. Y.-Z. Qian was supported by a grant at Caltech.

[1] See, for example, G. J. Mathews and J. J. Cowan, Nature (London) **345**, 491 (1990); K.-L. Kratz, J.-P. Bitouzet, F.-K. Thielemann, P. Möller, and B. Pfeiffer, Astrophys. J. **403**, 216 (1993).

[2] S. E. Woosley, J. R. Wilson, G. J. Mathews, R. D. Hoffman, and B. S. Meyer, Astrophys. J. **433**, 229 (1994).

[3] S. E. Woosley and R. D. Hoffman, Astrophys. J. **395**, 202 (1992).

[4] D. K. Nadyozhin and I. V. Panov, in *Proceedings of the International Symposium on Weak and Electromagnetic Interac-*

tions in Nuclei (WEIN-92), edited by Ts. D. Vylov (World Scientific, Singapore, 1993).
[5] K.-L. Kratz, F.-K. Thielemann, W. Hillebrandt, P. Möller, V. Harms, A. Wöhr, and J. W. Truran, J. Phys. G **14**, S331 (1988).
[6] G. M. Fuller and B. S. Meyer, Astrophys. J. **453**, 792 (1995).
[7] G. C. McLaughlin and G. M. Fuller, Astrophys. J. **464**, L143 (1996).
[8] G. V. Domogatskii and D. K. Nadëzhin, Sov. Astron. **22**, 297 (1978).
[9] G. C. McLaughlin and G. M. Fuller, Astrophys. J. **455**, 202 (1995).
[10] H.-T. Janka and W. Hillebrandt, Astron. Astrophys. **224**, 49 (1989).
[11] J. R. Wilson (private communication); and as cited in Y.-Z. Qian and G. M. Fuller, Phys. Rev. D **52**, 656 (1995).
[12] B. A. Brown and B. H. Wildenthal, Annu. Rev. Nucl. Part. Sci. **38**, 29 (1988); K. Langanke, D. J. Dean, P. B. Radha, Y. Alhassid, and S. E. Koonin, Phys. Rev. C **52**, 718 (1995).
[13] K. Nakayama, A. Pio Galeão, and F. Krmpotić, Phys. Lett. **114B**, 217 (1982).
[14] A. Gavron, in *Computational Nuclear Physics*, edited by K. Langanke, J. A. Maruhn, and S. E. Koonin (Springer-Verlag, New York, 1993), Vol. 2.
[15] P. Möller, J. R. Nix, W. D. Myers, and W. J. Swiatecki, At. Data Nucl. Data Tables **59**, 185 (1995).
[16] S. E. Woosley, D. H. Hartmann, R. D. Hoffman, and W. C. Haxton, Astrophys. J. **356**, 272 (1990); S. W. Bruenn and W. C. Haxton, *ibid.* **376**, 678 (1991).
[17] E. Kolbe, K. Langanke, S. Krewald, and F.-K. Thielemann, Phys. Rep. **227**, 37 (1993).
[18] T. W. Donnelly, J. Dubach, and W. C. Haxton, Nucl. Phys. **A251**, 353 (1975).
[19] See, J. Rapaport and E. Sugarbaker, Annu. Rev. Nucl. Part. Sci. **44**, 109 (1994) for a collection of (p,n)-measured GT-strength profiles.
[20] P. B. Radha, D. J. Dean, S. E. Koonin, and K. Langanke (in preparation).
[21] E. Kolbe, K. Langanke, S. Krewald, and F.-K. Thielemann, Nucl. Phys. **A540**, 599 (1992).
[22] Y.-Z. Qian and S. E. Woosley, Astrophys. J. **471**, 331 (1996); R. D. Hoffman, S. E. Woosley, and Y.-Z. Qian, *ibid.* (submitted).
[23] See for example, S. Goriely and M. Arnould, Astron. Astrophys. **312**, 327 (1996).
[24] P. Möller, J. R. Nix, and K.-L. Kratz, At Data Nucl. Data Tables (submitted).
[25] F. Käppeler, H. Beer, and K. Wisshak, Rep. Prog. Phys. **52**, 945 (1989).
[26] B. Chen, J. Dobaczewski, K.-L. Kratz, K. Langanke, B. Pfeiffer, F.-K. Thielemann, and P. Vogel, Phys. Lett. B **355**, 37 (1995).
[27] F. Käppeler, S. Jaag, Z. Y. Bao, and G. Reffo, Astrophys. J. **366**, 605 (1991).